On the propagation path of magma-filled dikes and hydrofractures: the competition between external stress, internal pressure, and crack length.

F. Maccaferri[1,2], D. Smittarello[3], V. Pinel[3], V. Cayol[4]

[1]GeoForschungsZentrum - GFZ, Potsdam, Germany.
[2]Istituto Nazionale di Geofisica e Vulcanologia - INGV, Osservatorio Vesuviano, Napoli, Italy.
[3]Univ. Grenoble Alpes, Univ. Savoie Mont Blanc, CNRS, IRD,IFSTTAR, ISTerre, 38000 Grenoble, France.
[4]Laboratoire Magmas et Volcans, UMR 6524, CNRS-IRD-Université Blaise Pascal, Clermont-Ferrand, France.
Corresponding author: Francesco Maccaferri (francesco.maccaferri@gfz-potsdam.de)

Key Points:

- We make use of analogue experiments and numerical simulations to study the propagation path of fluid-filled cracks in interaction with crustal stresses.
- We show and quantify how the competition between crustal stresses, fluid pressure, and crack length affect the path of fluid-filled cracks.
- We provide a critical range of values for a parameter which may help predicting the propagation path of a fluid-filled crack.

Abstract

Mixed-mode fluid-filled cracks represent a common means of fluid transport within the Earth's crust. They often show complex propagation paths which may be due to interaction with crustal heterogeneities or heterogeneous crustal stress. Previous experimental and numerical studies focus on the interplay between fluid overpressure and external stress, but neglect the effect of other crack parameters. In this study, we address the role of crack length on the propagation paths in presence of an external heterogeneous stress field. We make use of numerical simulations of magmatic dike and hydrofracture propagation, carried out using a two-dimensional boundary element model, and analogue experiments of air-filled crack propagation into a transparent gelatin block. We use a 3D finite element model to compute the stress field acting within the gelatin block, and perform a quantitative comparison between 2D numerical simulations and experiments. We show that, given the same ratio between external stress and fluid pressure, longer fluid-filled cracks are less sensitive to the background stress, and we quantify this effect on fluid-filled crack paths. Combining the magnitude of the external stress, the fluid pressure, and the crack length, we define a new parameter, which characterize two end member scenarios for the propagation path of a fluid-filled fracture. Our results have important implications for volcanological studies which aim to address the problem of complex trajectories of magmatic dikes (i.e. to forecast scenarios of new vents opening at volcanoes), but also have implications for studies that address the growth and propagation of natural and induced hydrofractures.

Plain Language Summary

Fluids move within the earth by means of different mechanisms. One of the most relevant mechanism, particularly for magma transport within the lithosphere, is the propagation through fluid-filled fractures: the fluid (or magma) can create its own path through the crustal rocks by fracturing them. If the density of the fluid is lower than the density of the rocks, the fluid would be pushed upwards by buoyancy (similarly to a gas bubble in water). However, the propagation path followed by these fluid-filled fractures may be complex. This may be due to several factors, including the forces (stresses) acting within the crust because of plate tectonic or because of remarkable topographic features. Here we make use of computer simulations and laboratory experiments to test how fluid-filled fractures interact with such crustal stresses. We quantify how

the competition between i) crustal stresses, ii) fluid (or magma) pressure, and iii) the length of a fluid-filled fracture, may affect its direction of propagation. We define a critical range of values for a parameter which may help identifying the path of a fluid-filled fracture propagating through the earth crust. Our results may have important implications for volcanological studies which aim to forecast scenarios of new eruption locations.

1 Introduction

Hydrofractures and magmatic dikes are mixed-mode fluid-filled cracks which may grow and propagate through the Earth's crust. A fluid-filled crack remains stable (it does not close and it does not grow nor propagate) as long as the stress intensity is positive and lower than the rock fracture toughness (*Weertman, 1971; Rubin and Pollard, 1987; Lister, 1990*). The same stability condition can be expressed by using the Griffith force (*Griffith, 1920*) or the total energy released during propagation (*Dahm, 2000a; Maccaferri et al., 2011*). These criteria apply when the hydrofracture propagation takes place within a "fracture-dominated" regime, which is defined based on the ratio between K_c - the rock fracture toughness - and K^* - a toughness scaling parameter that measure the viscous resistance to flow into the crack tip. Whether Kc/K* is greater or less than 1 means that the limiting factor in fracture propagation is either the resistance of the rock to failure (>1) or the resistance of the fluid to flow (<1) (c.f. *Rivalta et al., 2015* section 4.4). When $K_c/K^* >> 1$ the viscous resistance is negligible, and the Griffith or total energy criteria for the crack stability can be used to infer the most favourable direction for the crack growth (*Rivalta et al., 2015*).

A fluid-filled crack may become unstable if the excess of internal pressure is great enough, which can be due to buoyancy, possibly combined with stress gradients, or other sources of overpressure (e.g. connection to a magma chamber for magmatic dikes, or the injection of pressurised fluids for anthropic hydrofracturing operations). Hydrofractures and magmatic dikes often show curved and/or segmented propagation paths which may be due to interaction with crustal heterogeneities (e.g. faults, mechanical discontinuities in the rock properties, previous intrusions) or to heterogeneous crustal stress (which may be induced by topographic loads, for instance). In particular, there are clear geodetic evidences of late orientation changes or deflection of the ongoing trajectory for ascending dikes in volcanic edifices, where a spatial offset between the initially inflating area and the final vent is observed (eg, at Etna, Italy, *Bonaccorso et al, 2010*, at Piton de la Fournaise, Reunion Island, *Toutain et al., 1992*, *Peltier et al. 2005*, *Fukushima et al., 2010*, at Fernandina volcano, Galapagos, *Bagnardi et al, 2013*). Such deflections have been interpreted as controlled by the local stress field shaped by the surrounding topography (**e.g.** *Bonaccorso et al*, *2010*, *Corbi et al*, *2015*) and sometimes leads to a transition from vertical to lateral magma migration. The competition between vertical and lateral magma transport has also been studied theoretically considering an a priori fixed dike orientation (*Pinel & Jaupart, 2004*, *Townsend et al, 2017*). These studies show the influence of the local stress field on the ability of the magma to breach the surface and consequently on vents location. Besides, even in case of an horizontally dominated magma transport characterized by long dikes (several tens of kilometers), the dike orientation (or strike) is also clearly influenced by the local stress field resulting from the interplay between tectonic forces, magmatic reservoir overpressure and surface loading (**e.g.** *Meriaux & Lister, 2002*, *Grandin et al, 2009*, *Sigmundsson et al, 2015*, *Heimission et al, 2015*, *Roman & Jaupart, 2014*).

In general, fluid-filled cracks tend to propagate perpendicular to the local direction of the least compressive stress, given by the superposition of the background stress and the stress change induced by the intrusion (*Cotterell and Rice, 1980; Delaney et al., 1986*). This characteristic has been used to reconstruct the local stress field by observing the orientation of exposed dike intrusions (**e.g.** *Nakamura et al., 1977; Delaney et al., 1986*), or to forecast the propagation paths of magmatic intrusions given a model for the local stress field acting in the crust (**e.g.** *Corbi et al., 2016*). In so doing, the stress change due to the intrusion has been often neglected, sometimes leading to underestimates of paleo-stresses (*Meriaux and Lister, 2002*). Likewise, it has been shown that when dikes propagate into regions where the direction of the least compressive stresses is not perpendicular to the intrusion, they can travel significant distances before changing direction of propagation, and that they may even not be affected by the orientation of the external stress, if the magma pressure is large enough with respect to the magnitude of the external stress (*Watanabe et al., 2002; Menand et al., 2010*). In fact, in an elastic medium, the stress change induced by the opening of the fluid-filled crack would promote straight propagation along the crack plane. The actual crack path will depend on the relative magnitude of the background stress with respect to the stress change due to the intrusion, with the latter depending on the parameters characterizing the fluid-filled crack, such as the fluid overpressure (i.e. the excess fluid pressure with respect to the confining stress) and the crack length (*Cotterell and Rice, 1980*).

Watanabe et al. (2002), studied the competition between external stress and magma pressure by means of laboratory experiments, injecting oil-filled intrusions into a gelatin block. They applied a load on the surface of the gelatin, inducing a heterogeneous external stress field in the gelatin box, which was estimated by using analytical formula for the stresses in an elastic half-space subject to a surface normal load (*Jaeger et al., 2007, section 13.4*). They observed that only those intrusions with an internal pressure less than a certain value were deflected towards the applied load, following a propagation path perpendicular to the direction of the minimum compression. They computed a critical ratio for deflection (R_c) considering the ratio $R = \sigma_{xz} / Dp$ between the shear component of the external stress acting at the propagating tip of the intrusion (σ_{xz}) and the average overpressure of the intrusion (Dp). They found $R_c = 0.2$, meaning that intrusions with $R > R_c$ will be deflected towards the load while propagating to the surface.

In an other set of experiments, *Menand et al. (2010)*, used air injection into a gelatin block subject to lateral deviatoric compression to study the propagation path of fluid-filled crack in a compressive stress field. In their experiments the cracks are initially vertical and propagate upwards because of buoyancy. When the vertical air-filled crack is formed, a uniform lateral compression is applied to the gelatin. They observed a dike-to-sill rotation occurring only for large compressive stress or small buoyancy (i.e. when the ratio between the maximum overpressure and the horizontal compressive stress is smaller than 20). In addition, the response of the air-filled crack to the external stress was not instantaneous; they found that the distance needed by a vertical crack to turn to horizontal increased with the ratio of crack effective buoyancy to the compressive stress.

From a numerical modelling perspective, the problem of calculating magmatic dike trajectories has been addressed by different authors (e.g. *Dahm, 2000a; Meriaux and Jaupart, 2002; Maccaferri et al., 2011; Heimisson et al., 2015; Pinel et al., 2017*). Particularly, *Dahm (2000a) and Maccaferri et al. (2011)* reproduced similar results as obtained by *Watanabe et al. (2002)* for surface loading, and by *Menand et al. (2010)* in presence of horizontal compression.

These previous studies showed and quantified the competition between the fluid-filled fracture overpressure, and the magnitude of the background stress already present in the crust.-Therefore, given the external stress, the critical ratio for deflection computed by *Watanabe et al. (2002)*, defines the fluid-overpressure above which a fluid-filled crack does not turn to the direction perpendicular to the minimum compressive stress due to the background-stress. In contrast, if the overpressure is small enough, the crack will be deflected towards the direction perpendicular to the minimum compression. This critical ratio has been used to infer magma overpressure based on dike shallow trajectory evidenced by geodetic observations (*Bonaccorso et al., 2010; Corbi et al., 2015*).

Also, given a background stress model, the critical ratio for deflection represent an important reference value to validate forecast trajectories of magmatic intrusions (*Corbi et al., 2016*). Practically, the critical ratio for deflection, has been used to identify two end members scenarios for the propagation paths of the intrusions (*Pinel et al., 2017*): i) the total stress field is dominated by the background stress (the effect of the stress change due to the intrusion on its propagation path is negligible). In this case the trajectory of the intrusion is expected to follow closely the direction perpendicular to the least compressive background-stress axis; ii) the total stress field is dominated by the stress change induced by the fluid-filled crack (the effect of the background stress on the propagation path of the intrusion is negligible), in this case the fluid-filled crack would tend to propagate straight along the crack plane.

Previous experimental and numerical studies such as *Dahm, 2000a; Watanabe et al., 2002; Menand et al., 2010; Maccaferri et al., 2011*, focusing on the trade-off between internal overpressure and external stress, did not investigate the effect of the crack length on its propagation path. However, the magnitude of the stress change induced by the fluid-filled crack depends on the internal pressure and the crack length (*Segall, 2010*). In fact, given the same fluid overpressure, the magnitude of the stress change induced by the crack will scale with the crack length (the stress intensity factor is proportional to $L^{1/2}$). Given the same ratio (*R*) between the external shear stress acting at the upper tip of the crack (σ_{xz}) and the average overpressure of the fluid-filled crack (*Dp*), the propagation path of a fluid-filled crack should be affected by the crack length (*L*), as suggested by previous theoretical studies (*Cotterell and Rice, 1980; Meriaux and Lister, 2002*). In addition, recent studies focusing on the condition for lateral vs vertical propagation of magmatic intrusions, showed that the height of the crack plays a fundamental role in determining the location of the propagating front of the intrusion (*Townsend et al., 2017; Pollard and Townsend, 2018*). However, the effect of the crack length on the deflection of the intrusion has never been quantified separately from the effect of the internal pressure of the intrusion.

In this study, we address the issue of how the length of the intrusion affects the propagation path, in the presence of a heterogeneous external stress field. We revise the concept of critical ratio-for deflection previously introduced by *Watanabe et al. (2002)*, accounting for the crack length.

We make use of numerical simulations of fluid-filled crack propagation, carried out with a two-dimensional Boundary Element (BE) model (*Maccaferri et al., 2011*). This allow us to investigate a wide range of values of fluid overpressure and crack length. Furthermore, because numerical simulations are 2D, we performed new experiments of air-filled crack propagation into a transparent gelatin block, with a load applied at the surface. Both numerical simulations and laboratory experiments, have been performed with similar set-up as the one previously used by *Watanabe et al. (2002)*. In order to get more accurate and reliable estimate of σ_{xz}, we used a 3D finite element (FE) model to compute the stress field acting within the gelatin block (accounting also for the rigid boundaries of the box). Finally we perform a direct, quantitative comparison between our new experiments and the 2D numerical simulations. For this comparison we feed the BE model for dike propagation with a vertical cross section of the stress field acting in the gelatin block computed with the 3D FE model.

Our results may have important implications for all volcanological studies which aim to address the problem of complex trajectories of magmatic dikes (i.e. to forecast scenarios of new vents opening at volcanoes), and for studies that address the growth and propagation of natural and man-induced hydrofractures.

2 Methods

Both numerical and analogue experiments have been carried out with a set-up similar to the one used by *Watanabe et al. (2002)*: the intrusions start vertically oriented and when reaching the depth $z = 2.7\cdot(W/2)$, the load is applied at surface, at a horizontal distance $x = 2.8\cdot(W/2)$, between the crack tip and the centre of the load (where W is the width of the load, which is 6 cm for the analogue experiments). The geometrical set-up for the numerical and analogue experiments is shown in Fig. 1, distances (x^* and z^*) are normalized by the starting depth of the intrusion (z_s). The use of the same geometrical set-ups allowed a direct comparison between results obtained with different techniques (analogue and numerical), and between analogue experiments that used different fluids for the intrusion (*Watanabe et al., 2002* used silicon oil, we injected air).

We compute the loading stress by using analytical formulas for a uniform surface loading (*Jaeger et al., 2007*), when simulating magma-filled intrusions with BE model. However, in order to have a more precise estimate of the loading stress within the gelatin block, and when performing numerical simulations of the analogue experiments, we used a FE 3D stress model which accounts for the rigid boundaries of the tank. The FE calculation was performed with the commercial software COMSOL, applying a zero displacement condition at the lateral and bottom boundaries of the gelatin and using a mesh of around 200000 triangular units refined in a vertical plane centred below the load.

In both numerical simulations and analogue experiments we investigate the fluid-filled crack paths varying the ratio between the external shear stress acting at the tip of the crack and the average fluid overpressure R (1), the normalized length of the crack L^* (2), and the dimensionless parameter δ (3):

$$R = \sigma_{xz} / Dp \quad (1)$$

$$L^* = L / z_s \quad (2)$$

where z_s is starting depth of the intrusion.

$$\delta = R / L^* \quad (3)$$

Finally, we aim at providing an estimate for a critical range of δ-values (δ_c), which would characterize two end member propagation paths: $\delta < \delta_c$, straight propagation (small or no deflection due to the external stress); $\delta > \delta_c$, the propagation path follow closely the direction perpendicular to the least compressive stress axis of the background stress field.

2.1 Numerical model for fluid-filled fracture propagation

In order to quantitatively address the effect of crack length on the path of a fluid-filled fracture, we use a two-dimensional BE model (*Dahm, 2000a; Maccaferri et al., 2011*) to compute the trajectories of ascending intrusions. In our numerical simulations, the trajectories are obtained by incremental elongations of the crack in the direction that maximizes the elastic and gravitational energy release (*Maccaferri et al., 2011*). The intrusions are modelled as boundary-element mixed-mode cracks in plane-strain approximation, and are composed by N contiguous and interacting dislocations in an elastic half-space, with N in the range ~50-100 (simulations performed using 50 elements or more - up to 1000 - do not display any appreciable difference, Fig. S1). The fluid-filled crack opens and slips under normal and shear stresses constrains which are given by the fluid overpressure and by the shear component of the external stress field, respectively. The overpressure within the crack is defined as the difference between the fluid pressure and the normal component of the external stress (with respect to the orientation of each dislocation element). The fluid pressure profile is hydrostatic (linear and depth dependent), and the fluid density and pressure accounts for fluid compressibility. The external stress is the stress acting within the modelled crust, and results from the superposition of an isotropic, depth dependent, lithostatic stress ($\rho_r \cdot g \cdot z$, where ρ_r is the density of the host rocks, g is the acceleration due to gravity, and z is the depth), and the elastic stress induced by loading of the Earth surface (i.e. topography). This external stress field is responsible for the deflection of the intrusions towards the loaded region at surface, following different trajectories depending on the magnitude of the loading, the fluid overpressure, and the crack length.

In our model we consider the propagation of initially vertical fluid-filled cracks with vanishing stress intensity factor at the lower tip (*Weertman, 1971*). The initial average fluid overpressure (Dp) is proportional to $\Delta\rho$ and L (where $\Delta\rho = \rho_r - \rho_f$ is the difference between rock and fluid densities). We increase the starting overpressure either by increasing the starting length of the crack, or by decreasing the density of the fluid. The starting length of the fluid-filled crack, is constrained by the cross sectional area of the crack (2D volume of the intrusion), which is given as an input parameter to the numerical simulations.

The model parameters are set with average characteristic values for magmatic dike intrusions propagating through the earth crust: we set the density of rock between 2000 - 2500 kg/m^3, rigidity and Poisson's ratio to 20 GPa and 0.25 respectively, magma density and bulk modulus between 2000-2450 kg/m^3 and 10-25 GPa, respectively. We also tested lower fluid density (1200 kg/m^3), which would be in the range of values for hydrofractures. The loading pressure ranges between ~2-10 MPa, and the width of the loading plate between 0.5 - 10 km (c.f. Tab S1).

In addition, we simulated 5 of the analogue experiments (exp34, 35, 44, 59, and 61) with the BE model for dike propagation. In this case we set the model parameters with the values we measured in the laboratory.

2.2 Laboratory technique

We performed experiments of air-filled crack propagation into a transparent brittle-elastic gelatin block. The experiments where performed in the “Bubble Lab” at the German Research Centre for Geoscience (GFZ), in Potsdam, Germany. We used a plexiglas tank of 40×20×20 cm and a loading plate with variable weight, with rectangular base of 14x6 cm (see Fig.1b). The tank was filled with 16 L of gelatin with a concentration of 2% by weight. The gelatin cooled at ambient temperature until 33° C then was put in a fridge for 20 h at a temperature of 5° C. We assume that the Poisson's ratio for gelatin is 0.5 (*Kavanagh et al., 2013*). We estimated the gelatin rigidity (*E*) by measuring the maximum vertical displacement at the surface due to the loading, and comparing it with the one obtained with the FE model of the gelatin block. We estimate *E* to be 3500 Pa, without significant variations from one day to an other.

We injected a controlled volume of air with a syringe from different holes at the base of the tank. A sheet-like, air-filled crack formed and started propagating upwards due to buoyancy. When the intrusion reached the starting depth, the loading mass was put on the surface of the gelatin block, at the desired horizontal distance. Each propagation experiment had a duration that could vary between a few seconds up to a few minutes, depending on the injected volume (the larger the volume, the shorter the experiment duration).

To investigate the effect of crack length on the propagation path, a good a-priori estimate of the ratio *R* between external stress and fluid overpressure was required. Such an estimate allowed us to plan and perform experiments with similar *R*, but different crack lengths. The average overpressure *Dp* within a fluid-filled crack depends on the crack length, for a given density contrast between intrusion and host material ($\Delta\rho = \rho_{gel} - \rho_{air} \simeq \rho_{gel}$ is constant and equal to 1.0 g/cm^3 in our experiments):

$$Dp = (\rho_{gel} \cdot g \cdot L) / 4 \quad (4)$$

(*Watanabe et al., 2002*)

We performed 23 calibration experiments to get an empirical relationship between the injected volumes and the corresponding crack length, for our experimental set-up. Using eq. (4), we could estimate the average overpressure within the crack, for a given injected volume. In this way we could choose the loading mass needed to obtain the desired ratio $R = \sigma_{xz}/Dp$, since the external shear stress is proportional to the loading mass applied at surface. This procedure was used to obtain an a priori estimate of *R*. However, after each experiment, *R* has been computed according to the actual length of the crack and to the shear stress acting at its upper tip.

In total, we performed 62 experiments (including the calibration experiments) during 3 weeks. 14 of them failed (mainly because of air-leakages during the injection, or because the air-filled crack reached a previous fracture while forming). We conducted 25 deflection experiments with different volumes and different loading masses. We recorded the path of the intrusion with 3 cameras, a front view (cross section) a lateral view and a top view (Fig. 1c). The camera records have been analysed with the software TRACKER (https://physlets.org/tracker/). By tracking the position of the propagating tip of the air-filled crack we could deduce its trajectory. From the camera records we also measured the actual length, width, strike, dip angle, and relative position of the air-filled crack with respect to the loading mass, when the load was put onto the gelatin block. This allowed us to check the accuracy of the initial conditions for each experiment. Among the 25 deflection experiments, 10 of them were discarded because of inaccurate initial conditions, either on the initial strike orientation or on the initial dip angle. In the 15 selected experiments, all intrusions strike approximately parallel to the long edge of the loading mass (strike angles range from -14° to 12°, with respect to the long edge of the load, c.f. Tab. 1), and have almost vertical initial dip angles (dip angle deviations from the vertical are between -3.5° and 3.5°, c.f. Tab. 1).

The observed initial crack-length (when the deflection experiment starts) has been used to compute the actual overpressure *Dp* within the crack. For each experiment, the initial position of the loading mass with respect to the tip of the intrusion, has been used to compute the actual external shear stress σ_{xz} acting within the gelatin block, at the tip of the crack. In this way we measured the actual ratio *R* between the air-filled crack overpressure and the shear stress induced by the loading at the tip of the crack.

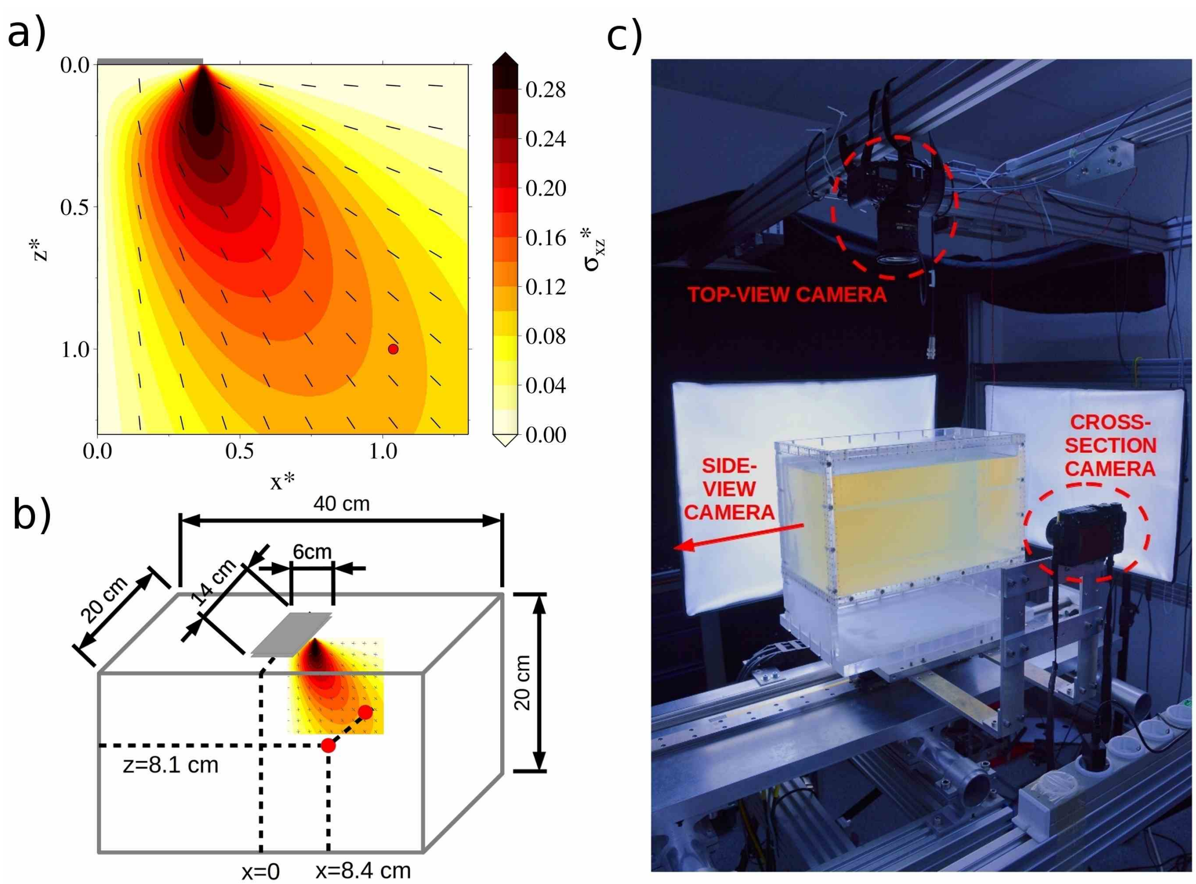

Figure 1: *Numerical and experimental set-up. a) Numerical model set up: the gray segment at z* = 0 represent half of the loading mass, the red dot marks the starting position of the upper tip of the propagating fluid-filled crack, the black segments indicate the direction of maximum compression, the coloured contour is the shear stress induced by the loading, normalized by the loading pressure. Here the stress field has been computed with analytical formulas for a vertical load at the surface of an infinite half-space (*Jaeger et al., 2007*). b) Sketch of the gelatin container, the red dot marks the position of the upper tip of the air-filled crack at the moment of applying the loading onto the gelatin block. c) Photo of the laboratory setting.*

3 Results

3.1 Results from numerical simulations of magmatic dike propagation

The simulations we show in this section display how fluid-filled crack paths change depending on *R*, *L**, and δ, as they have been defined in eq. (1), (2) and (3).

We first present results from a set of simulations where we vary the ratio R by applying constant loading (constant σ_{xz}) and different magma average overpressure (*Dp*). We obtain progressively more deflected paths with decreasing magma overpressure (Fig. 2a), which is in agreement with results from previous analogue experiments and numerical simulations (*Dahm, 2000a; Watanabe et al., 2002*). In this set of simulations we use a constant fluid density, and increase *Dp* by increasing the initial length of the intrusion.

In order to isolate the effect of the dike length we run a second set of simulations with constant ratio *R*, but with different starting lengths *L**. We obtain progressively more deflected paths for smaller initial dike lengths (Fig. 2b). Here *R* is kept constant by keeping constant both σ_{xz} and *Dp*. We vary the initial dike length and set the fluid density so that $R = 0.11$ for all simulations.

In the third set of numerical simulations we consider loading masses, dike overpressures, and dike lengths, such that the quantity δ is constant. We find that dike trajectories with different lengths *L** and different ratios *R* tend to get close to each other if δ is constant (Fig. 2c). However, a drift towards more deflected trajectories is now appreciable for increasing *L** (and therefore increasing *R*).

Finally, we identified a combination of parameters for which dike trajectories obtained with different *Dp* and *L* overlaps almost exactly (Fig. 2d). In this set of numerical simulations we keep *R* and *L** constant, and vary *Dp* and *L*. This has been obtained by changing the loading pressure (i.e. σ_{xz}), the fluid density, and the dike starting depth (z_s) according to $R = 0.11$ and $L^* = 0.74$. Here we also varied the load width *W* in order to have constant normalized width $W^* = W/z_s$ in all simulations.

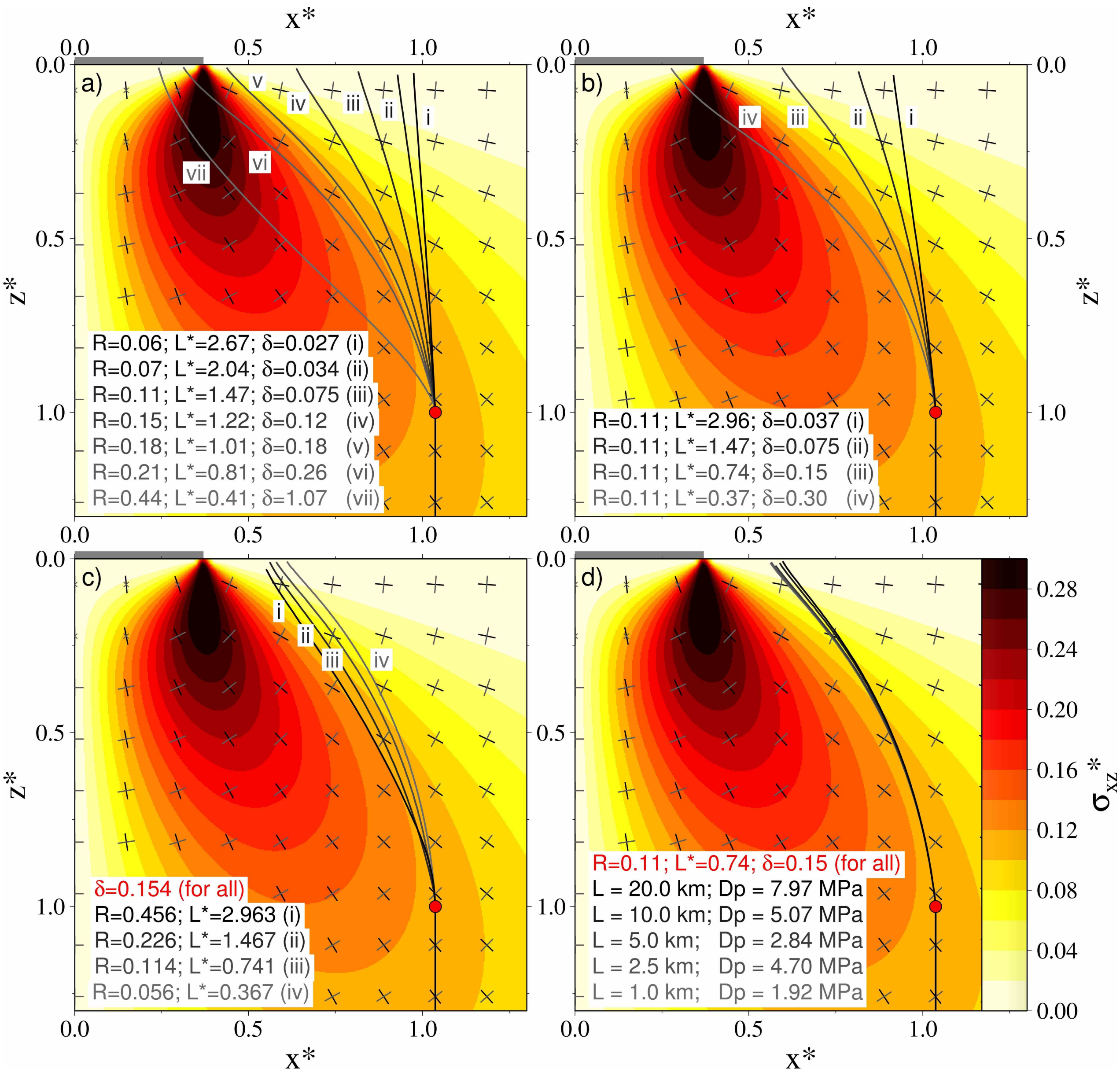

Figure 2: *Simulated fluid-filled crack paths. Black segments indicate the direction of maximum compression, gray segments the minimum compression (the small crosses beneath the loading indicate the out-of-plane direction). Colour contours are the same as Fig. 1. All lengths are normalized by the starting depth of the crack tip. The gray segment at $z^* = 0$ represents the normalized half-width of the loading ($W^*/2 = 0.37$). Fluid-filled cracks start vertically oriented with the crack tip position indicated by the red dot. The crack paths are marked by the solid lines. Panel a) Fluid-filled crack paths obtained with increasing R. b) Paths obtained with constant R and decreasing L^*. c) Paths obtained with constant δ. d) Paths obtained with constant R and L^*.*

3.2 Results from analogue experiments

Here we show results from 15 deflection experiments which had the best initial conditions for dip and strike angles (c.f. Tab. S2 for the list of all experiments). The parameters characterizing each experiment are listed in Tab. 1.

We first compare air-filled crack trajectories which have similar normalized length L^* and different ratios R (Fig. 3), which would reproduce results similar to those discussed in *Watanabe et al. (2002)*. Then we compare trajectories for air-filled cracks with similar R and different L^* (Fig. 4), to show the influence of L, similarly to our numerical simulations in Fig. 2b. Finally we compare trajectories sorting them according to their δ values (Fig. 5), similarly to our simulations in Fig. 2a, and estimate a critical range of δ values, δ_c.

Exp #	Loading Mass (g)	Dip dev. (degrees)	Strike (degrees)	x_s (cm)	z_s (cm)	L (cm)	L*	σ^*_{xz}	R	δ
29	181.0	-1.2	-9.5	10.0	6.6	6.1	0.94	0.036	0.050	0.053
30	110.5	-1.1	5.1	7.9	8.6	3.6	0.42	0.062	0.088	0.208
31	166.0	-0.5	9.5	8.5	7.6	5.5	0.73	0.058	0.081	0.112
34	127.0	1.1	0.2	9.7	8.5	3.2	0.38	0.044	0.082	0.216
35	194.0	1.8	-3.6	8.4	8.3	5.6	0.68	0.058	0.095	0.139
38	222.0	0.2	3.9	8.3	10.5	6.2	0.59	0.050	0.084	0.144
42	64.0	2.6	11.6	8.6	8.5	3.6	0.42	0.057	0.049	0.116
43	38.0	3.4	-4.2	9.8	8.4	3.7	0.44	0.043	0.021	0.048
44	25.4	1.1	-14.1	9.7	8.6	3.3	0.39	0.042	0.015	0.039
45	171.9	0.1	2.4	8.7	7.5	5.6	0.74	0.054	0.079	0.106
49	96.8	-0.2	1.1	9.3	7.9	5.6	0.71	0.050	0.041	0.058
50	81.4	2.4	8.1	7.9	8.1	4.8	0.60	0.065	0.053	0.089
59	111.9	0.1	-6.3	8.6	8.4	4.5	0.54	0.055	0.064	0.120
60	262.9	-0.8	-2.5	9.4	8.7	4.5	0.51	0.045	0.126	0.247
61	229.6	-0.2	0.7	9.0	8.6	3.8	0.44	0.051	0.146	0.332

Table 1: *Relevant parameters for the experiments considered in the current study. Note that "Dip dev." is the initial deviation of the air-filled crack from a vertical dip angle (positive angles pointing towards the load, negative outwards). The "Strike" is taken with respect to the direction of the long edge of the loading plate (positive clockwise).* σ^*_{xz} *is the shear stress acting at the tip of the crack at the beginning of the deflection experiment normalized by the loading pressure.*

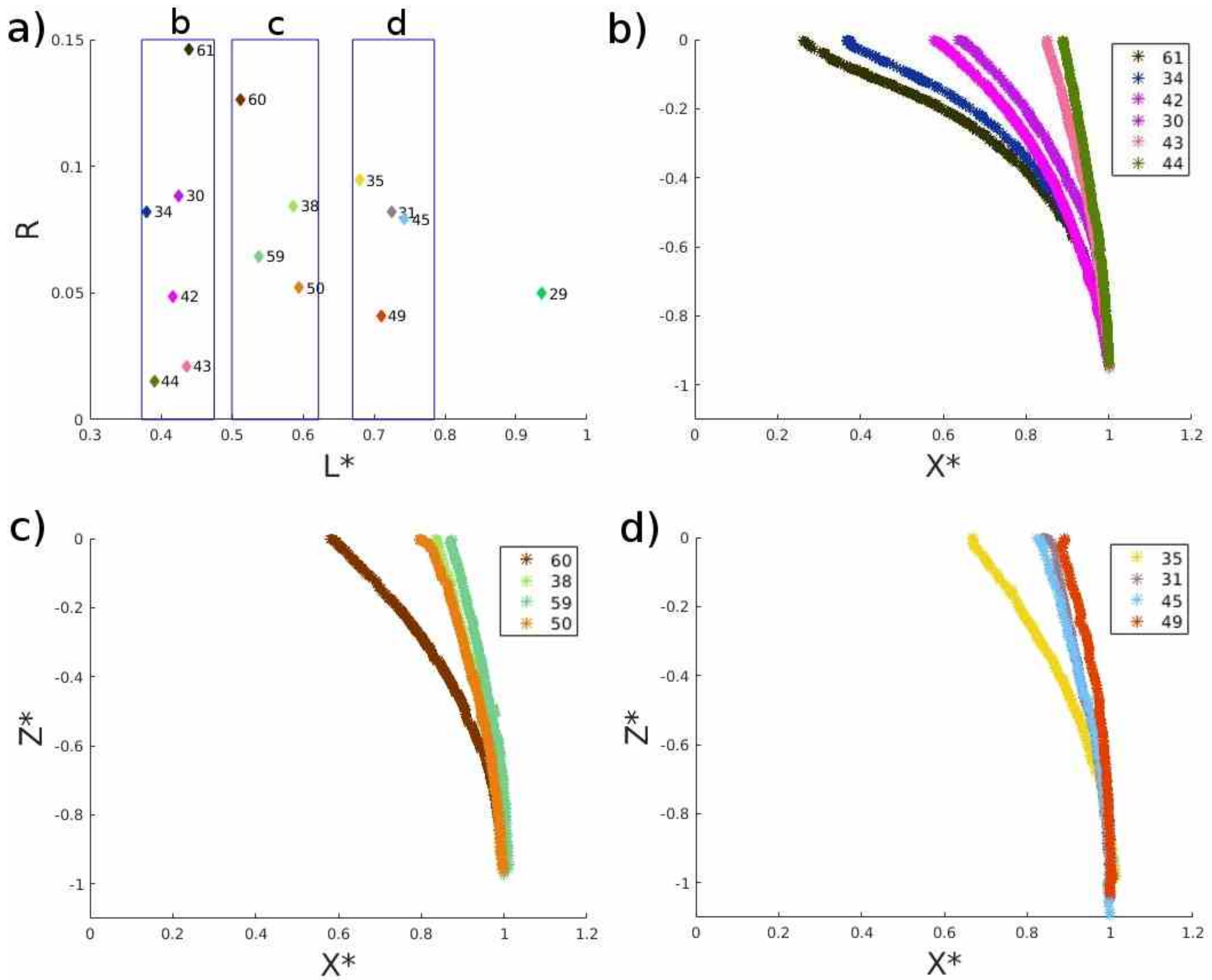

Figure 3: *Air-filled crack paths within the gelatin block digitized from the experiment records. In this figure we compare paths followed by cracks with similar L* and different R. Panel a) Scatter plots of the ratio R versus the crack length L* for each experiment. Rectangles highlight three groups of experiments with similar crack lengths. Panels b-c-d) Trajectories of experiments belonging to the first, second, and third rectangle, respectively.*

In Fig. 3a we plot the values of R vs L^*, and identified 3 families of experiments with similar L^* (blue rectangles). Air-filled crack trajectories are plotted in Fig. 3b-c-d. All trajectories, within each L^* range, are generally more deflected as R is higher, as expected. Only two trajectories deviate from this trend, and they can be explained considering the initial conditions of those experiments: Exp30 appears to be less deflected than expected, this may be due to the fact that exp30 is the only one which has an initial negative dip angle deviation (outward dipping, with respect to the loading), among all the other experiments in Fig 3b (cf. Tab 1). Exp50 (Fig. 3c) is slightly more deflected than expected, and has a larger initial dip angle deviation (2.4°) with respect to the other intrusions in Fig. 3c (0.2°, 0.1°, -0.8° for exp38, exp59 and exp60 respectively). Despite these differences on the initial dip angle, the effect of the ratio R on the amount of deflection appears clear.

In order to check the influence of the crack length on the trajectories of the air-filled cracks, we select experiments with similar ratios R and different lengths L^* (Fig. 4a, red rectangles). The four experiments with $R \simeq 0.045$ ($0.041 > R > 0.050$) display greater deflection for shorter L^*, Fig. 4b, in agreement with the results from numerical simulations (Fig. 2b).

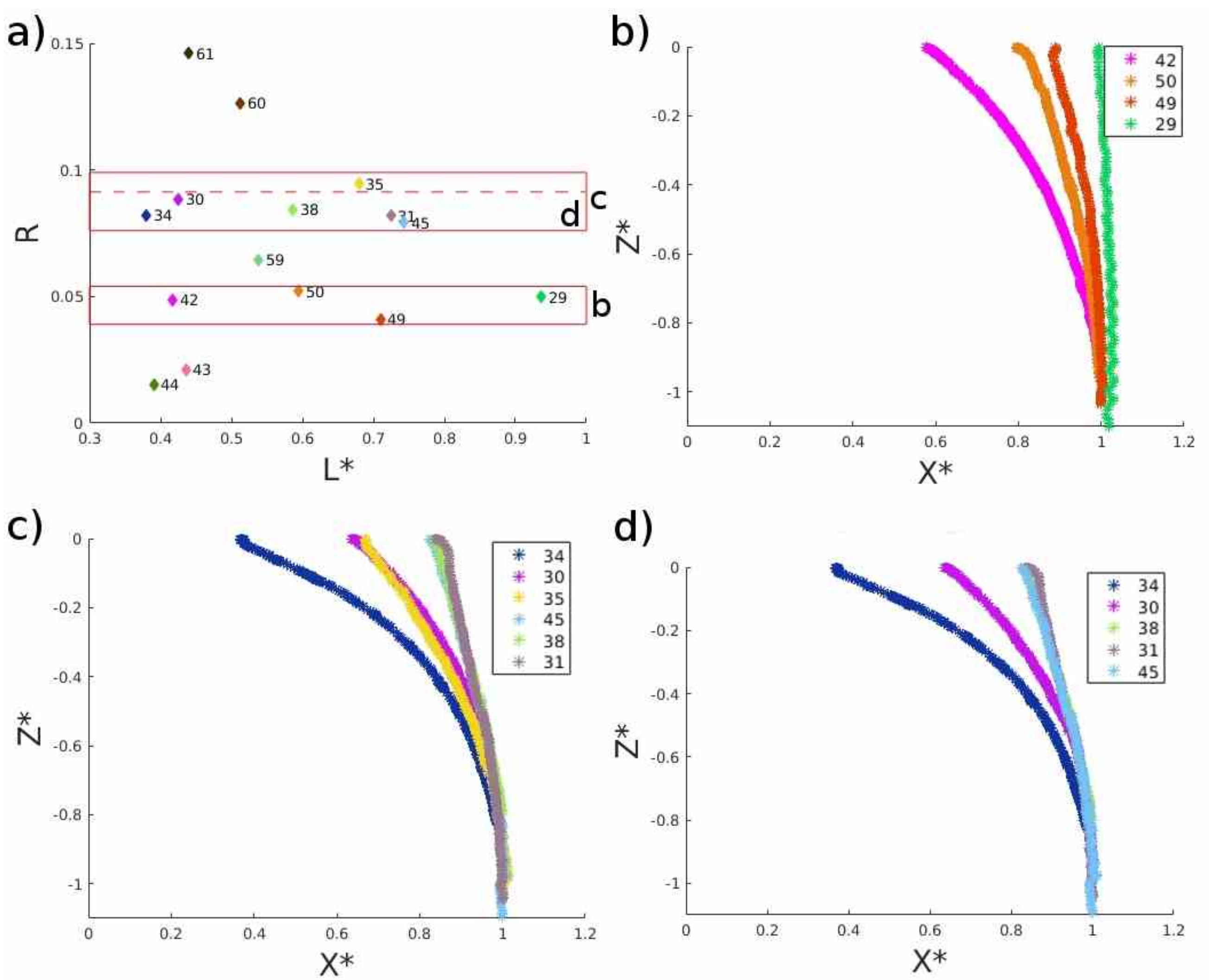

Figure 4: *Experimental paths followed by cracks with similar R and different L*. Panel a) Scatter plots of the ratio R versus the crack length L* for each experiment. Rectangles highlight two groups of experiments with similar crack R. Panels b-c) Trajectories of experiments belonging to the first and second rectangle, respectively. Panel d) Same as c) but excluding experiment 35.*

For the second set of experiments, with $R \simeq 0.085$ ($0.079 > R > 0.095$), Fig. 4c, the same trend is generally confirmed, however the trajectory of exp35 display a greater deflection than expected, considering that its initial crack length L^*. Noticeably, the R value of exp35 ($R = 0.095$) is at the upper edge of the range we selected, therefore its greater deflection may be due to the influence of R dominating over the effect of L^*. In fact, by narrowing the range of R to $0.079 > \mathrm{R} > 0.088$, we find the expected trend of decreasing deflection for longer L^*, Fig. 4d. This may indicate that trajectories are more sensitive to the value of *R*, so that in order to highlight the effect of *L** it is necessary to select experiments with *R* values within a narrower range, e.g. < 0.01.

In addition, we note that the trajectories of exp38, exp45 and exp31 overlap, even though the cracks in exp45 and exp31 are longer than the one in exp38. However, all of them display very little deflection, which may indicate that the sensitivity of deflection to crack length is depressed at crack lengths greater than in exp38 (within this range of *R* values).

Initial dip angles also affect the amount of deflection, and it is worth mentioning that the air-filled cracks in exp30 and exp34 have opposite initial dip angle deviations (-1.1° and +1.1°, respectively) and this may cause trajectories to diverge more from each other. Exp35 has the greatest positive initial dip angle in Fig.4c, and this may contribute to its deflection being greater than expected. We discuss in further details the effect of initial dip angle deviations in section 4.2, paragraph "Experimental conditions".

Finally, we sorted our experiments according to δ, in order to check whether this parameter is able to characterize the deflection of an intrusion, accounting for the effect of both *R* and *L**. If this is true, we should be able to identify a critical value (or range of values) of δ above which all intrusions are effectively deflected, and below which all intrusions are not or poorly deflected. Given the geometry of our experimental set-up, the amount of deflection can be quantified by the ratio between the horizontal and the vertical distances travelled by the air-filled crack tip: $\Delta = \Delta x/\Delta z$. Experiments in Fig. 5b show the overall greatest deflections ($0.4 < \Delta < 0.8$), and they are associated with values of $\delta > 0.2$. In contrast, all experiments with $\delta < 0.06$ (Fig. 5d) display very little or no deflection ($\Delta < 0.1$). Experiments with intermediate δ values (Fig. 5c) display more scattered trajectories, consistently lying in between the ones in Fig. 5b and Fig. 5d ($0.1 < \Delta < 0.4$), as it may be expected for intrusions characterized by δ values within the critical range δ_c.

The experimental paths in Fig. 5 show that δ may be a suitable parameter to characterize two end member trajectories: straight propagation (or with very small deflection, i.e. $\Delta < 0.1$) which will correspond to $\delta < \delta_c$; and propagation close to the direction perpendicular to the least compressive stress due to the load (which we obtained in exp34 and exp61, which display $\Delta > 0.6$). We estimate the critical range δ_c=[0.06; 0.22] which is obtained considering the higher δ value for the lesser deflected experiments (c.f. Fig. 5d, exp49, with $\Delta \sim 0.1$), and the lower δ value for the most deflected experiments (c.f. Fig. 5a, exp34, with $\Delta \sim 0.6$).

Looking into some further details, we noticed that trajectories of exp30 and exp60 (Fig. 5b) are very similar, and those experiments have similar δ and initial dip angles (deviating from vertical of -1.1°, and -0.8° respectively). Exp34 (Fig. 5b) is more deflected, however it has a positive initial dip angle deviation (1.1°). Moreover, exp31, exp38, exp45 and exp59 (Fig.5c) have similar δ values and initial dip angles (deviations of -0.5, 0.2°, 0.1°, and 0.1° respectively), they indeed display very similar paths. Exp35 and exp42 (Fig.5c) have also similar δ and similar larger dip angle deviations (1.8° and 2.6° respectively), their paths are similar. Exp50 is less deflected, even if it has an initial dip angle deviation of 2.4°, however it also has the lowest δ value within the range considered in Fig. 5c. This is in agreement with results from the numerical model, which show similar paths for intrusions with the same δ value (given the same initial conditions).

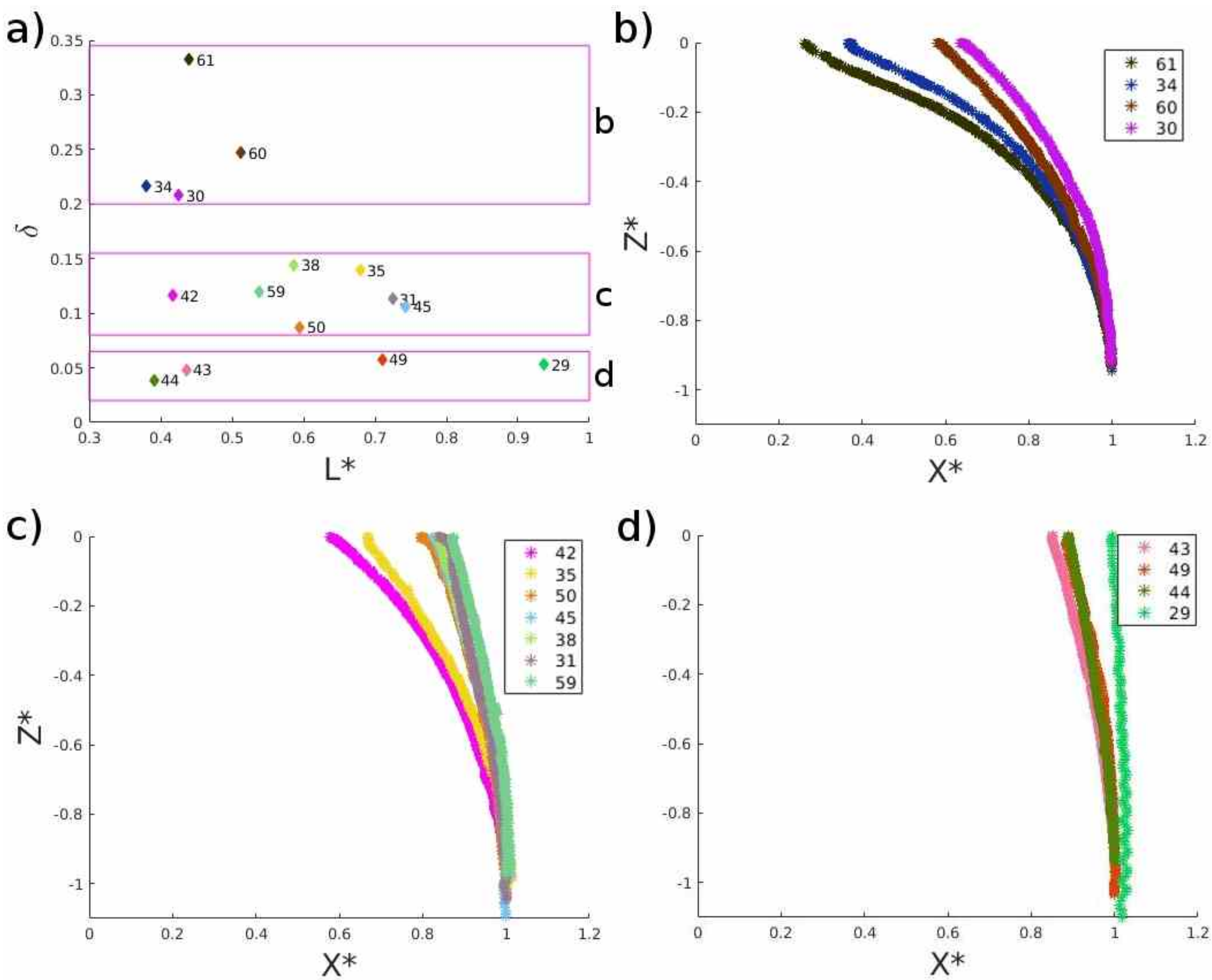

Figure 5: *Experimental paths followed by cracks with similar δ. Panel a) Dispersion plots of δ values versus L*. Rectangles highlight three groups of experiments with different δ. Panels b, c, d) Trajectories of experiments belonging to specific rectangles, with δ > 0.2, 0.08 < δ < 0.15 and δ < 0.06 respectively.*

3.3 Comparison with previous analogue experiments from *Watanabe et al., 2002*.

In order to calculate the ratio *R* for each deflection experiment, we computed the stress field acting within the gelatin block with a 3D FE model. We compared the stress field computed with 2D analytical formula in plane strain approximation for a semi infinite elastic medium (*Jaeger et al., 2007*), Fig. 6a, with the one obtained with the FE model, Fig. 6b. Our results show a significant difference in the magnitude of the shear stress due to surface loading, demonstrating the importance of considering realistic boundary conditions when evaluating stress fields within the gelatin block. In particular, the shear stress σ_{xz} acting at the starting position of the upper tip of the air-filled crack is a factor ~0.5 smaller in the 3D FE calculation, compared to the analytical one (σ^*_{xz} = 0.06 and σ^*_{xz} = 0.11, respectively). Considering the analytical stress, instead of the FE one, results in overestimating the loading stress acting within the gelatin block, thus directly affecting the estimate of *R*, and δ.

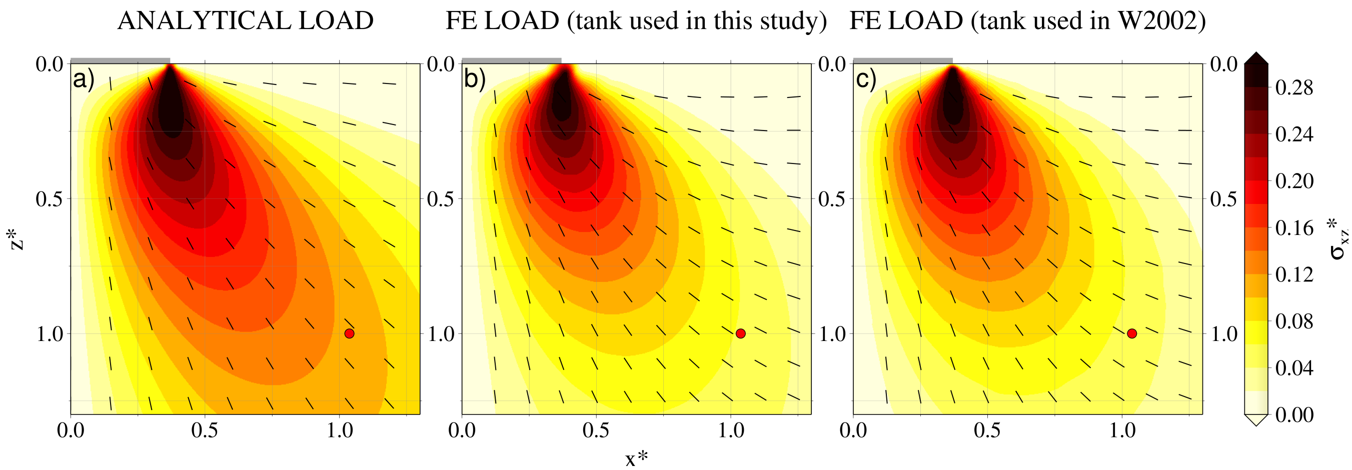

Figure 6: *Loading stress as computed by a) analytical formulas for an infinite medium (Jaeger et al., 2007), used in Watanabe et al. (2002). Note that here the in-plane stress field does not depend on the Poisson's ratio, b) FE model of the gelatin block with rigid boundaries and dimensions of the tank used for the present study, c) FE model of the gelatin block with rigid boundaries and dimensions of the tank used by Watanabe et al., (2002). For the FE models we used a Poisson's ratio ν = 0.49. Coloured contours are the same as Fig. 1.*

The critical ratio for deflection R_c = 0.2 given in *Watanabe et al. (2002)*, has been computed considering analytical stress calculation (Fig. 6a). Our calculations for the stress field within a gelatin block with the same dimensions as the ones specified in *Watanabe et al. (2002)* (Fig. 6c), would result in a lower critical ratio for deflection R_c = 0.09 (considering the experiments run by *Watanabe et al., 2002*). This ratio, however, does not consider the effect of *L** on the propagation path of the crack. Considering the crack lengths given in *Watanabe et al. (2002)* for those experiments, we can estimate the critical range of values δ_c. We computed δ_c=[0.10; 0.17] (obtained considering the trajectories of the experiments relative to Dp/P_{load} = 0.53 and 0.60, and Dp/P_{load} = 0.23 and 0.30, in *Watanabe et al., 2002*, Fig. 5b and 5c therein, respectively). Such critical range of values for δ is within the one we computed from our experiments, which is between 0.06 and 0.22.

3.4 Comparison between analogue experiments and numerical simulations

The simulated dike trajectories systematically show greater deflections than experiments, given the same values of *R* and *L**. From the numerical simulations in Fig. 2a and 2b we can estimate a critical range for δ values δ_c=[0.037; 0.18], since non- or very poorly deflected trajectories (with deflection Δ < 0.1, paths i and ii, in Fig. 2a and path i in Fig. 2b) are obtained for δ < 0.037, and effective deflections (Δ > 0.6, paths v, vi, and vii, in Fig. 2a) are found for δ > 0.18.

We performed a direct comparison between experiments 35, 44, 59, and 61, which span a range of δ parameters between 0.04 to 0.33. We set-up the numerical simulations with the intrusion parameters corresponding to each of those experiments (Tab. 1). For these simulations we used the loading stress field computed with a FE model (Fig. 6b). In general, the simulated trajectories (solid black path in Fig. 7) are more deflected than the experimental paths (gray dashed path, Fig. 7). The only simulation that exactly reproduces the experimental path is exp44 (Fig. 7d). In this experiment δ = 0.04 is at the lower bound of δ_c estimated from both, experiments and simulations.

A good match is also obtained for the arrival position at the surface in exp61 (δ = 0.33, Fig. 7a). However, in first part of the propagation path, the simulated path diverges from the experimental one (which is less deflected). Simulated and experimental paths proceed parallel until they reach the vicinity of the surface. Then, both paths converge to a similar location. In this experiment δ is larger than the upper bound of δ_c estimated from both experiments and numerical models. The two experiments with intermediate δ values, exp35 and exp59, δ = 0.14 and δ = 0.12 (Fig. 7b and 7c) respectively, show the greatest difference between numerical and experimental paths. In these two experiments δ is within the range of critical values estimated from the experiments and from the numerical simulations.

The reasons for the differences between experiments and simulations will be discussed in the following section.

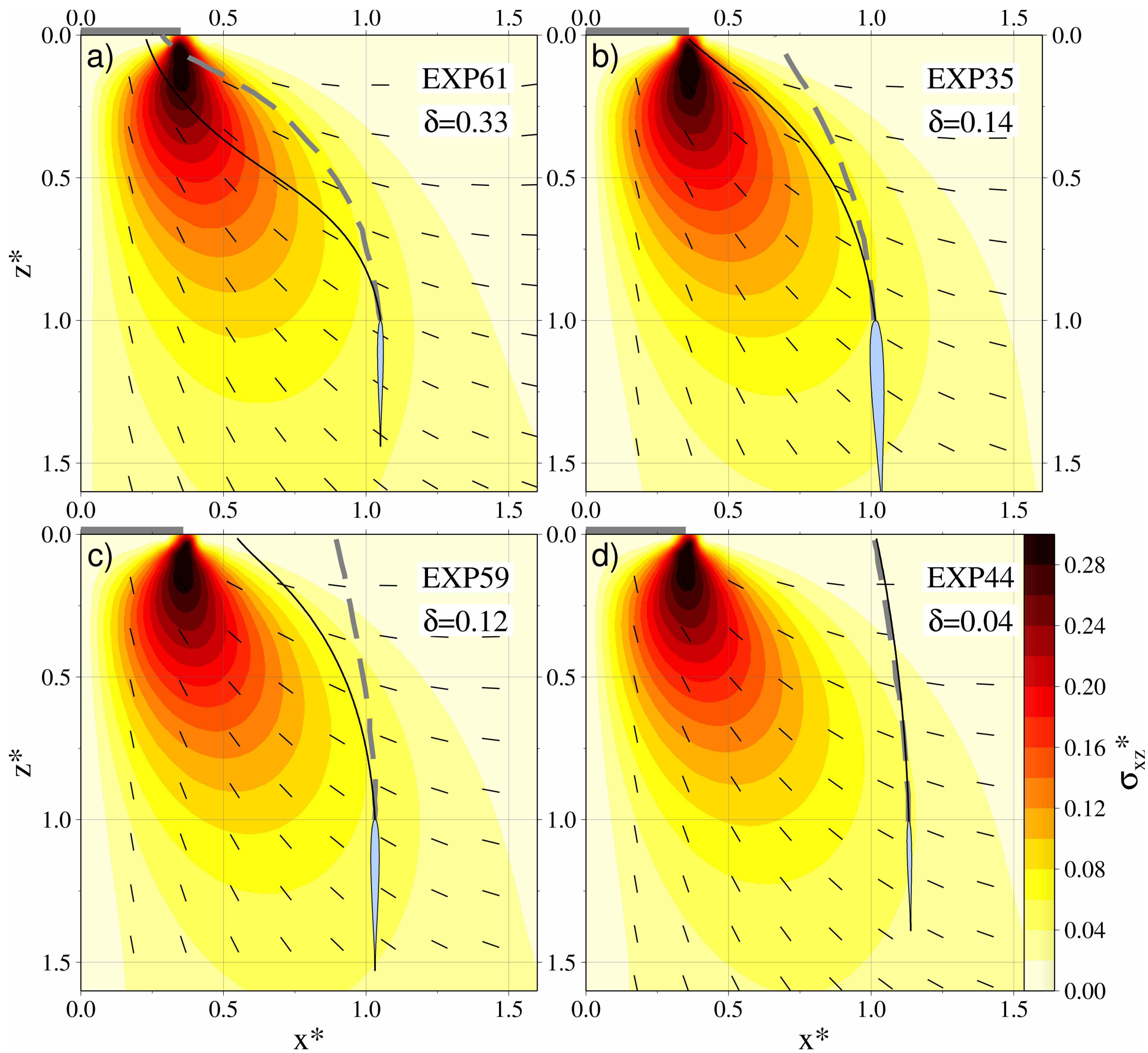

Figure 7: *Numerical simulations of 4 analogue experiments. Numerical paths are the black solid lines, experimental paths are the gray dashed lines. The loading stress is computed by a FE model of the gelatin block (Fig. 6b). Colour contours in different panels are slightly different because the starting depth z_s, which are used to normalize lengths in each plot, are slightly different for each experiments. Coloured contours are the same as Fig. 1, 2, and 6.*

4 Discussion

4.1 The critical range of delta and propagation scenarios

We introduced a new parameter (δ) accounting for the crack overpressure, length and magnitude of the external stress, and estimate a critical range of values (δ_c), based on which we define three possible propagation scenarios characterized by $\delta>\delta_c$, $\delta<\delta_c$, and $\delta\in\delta_c$. In the first case the propagation path is dominated by the background stress (i.e. the contribution to the total stress due to the stress change induced by the intrusion is negligible), and the trajectory is expected to follow closely the direction perpendicular to the less compressive stress induced by the background stress field. In the second scenario, the stress change induced by the fluid-filled crack dominates (the effect of the background stress on the propagation path is negligible), and the intrusion is expected to propagate straight or be poorly deflected. When δ values are within the critical range, the path of the fluid-filled fracture will be in between the two end member trajectories described above. Both, background stress and stress change due to the intrusion give a non-negligible contribution to the propagation path, and computing trajectories will require specific and more complex models which simulate the propagation path accounting for the interaction of the intrusion with the background stress.

4.2 Differences between numerical simulations and experiments

By using the BE model for dike propagation, we explored a wide range of material properties and parameters characterizing the intrusions. However, the numerical model relies on a 2D assumption which in our view represents its major limitation. For this reason we performed a number of analogue experiments. We focused our experimental analysis on varying the air-filled crack overpressure and length as much as we could. Given the limitations imposed by the experimental conditions we could vary the crack length between ~3 to ~6 cm (air-filled cracks smaller than 3 cm length were not propagating, and above ~6 cm were too fast to be able to control the positioning of the loading mass at surface).

By joining these two techniques, we aim to take the maximum possible advantage from both the numerical and analogue experiments (and at least partially overcome their limitations). A necessary condition for achieving such an aim, is that results obtained with the two techniques are consistent with each other. This appears to be partially true, although some discrepancies are displayed in the numerical simulations of analogue experiments 35, 44, 59, and 61. The simulated air-filled cracks are more sensitive to the external stress field, or conversely, the experimental air-filled cracks need more distance (or time), to adjust towards the direction of maximum compression. This leads to different estimates for δ_c derived from analogue experiments and numerical simulations. Several factors may contribute to these differences:

- *3D effects*: The BE model uses the plane-strain approximation, implying that the modelled cross section of the intrusion extend to infinity in the out of plane direction. Neglecting the 3D shape of the air-filled crack may introduce differences in the propagation path. In particular, the unbounded width of the crack may introduce differences with respect to the self induced stress due to a 3D fluid-filled crack with finite width. Two competing effects may act: On one hand, the self induced stress of the plane strain crack should be larger than the one induced by a finite 3D crack. This would cause even lesser deflection of a plane-strain crack compared with a 3D crack, while we observe the opposite. On the other hand air-filled cracks have a rounded shape of the propagating tip in the out-of-plane direction which is neglected in the BE model. This geometry may increase the energy spent for bending the crack tip out of the crack plane, with respect to the plane strain crack approximation, making the 3D crack less responsive to the external stress. Overall, since there are no 3D models for the propagation path of a fluid-filled crack, we cannot quantify the respective role of both factors and the final effect of the 2D approximation.

- *Fluid viscosity*: The BE model uses a "quasi-static" approach. In this, the crack propagation is simulated by elongating the crack and solving the fluid-filled crack problem at static equilibrium. The lower tip of a static, buoyant, fluid-filled crack closes with vanishing stress intensity factor (*Weertman, 1971*). However, models that account for the dynamic effects of viscous flow within moving cracks, predict an open tail with thickness which depends on the fluid viscosity (e.g. *Dahm, 2000b; Roper and Lister, 2007*). Propagating air-filled cracks, though, do not display such open tail, and the crack thins and completely closes at the lower tip (probably because of the very low viscosity of air, $\sim 1.8\times10^{-7}$ Pa·s). Therefore, we do not expect the air flow to sensibly lower the average overpressure of the propagating air-filled crack, with respect to a static one. However, more generally, the air-flow within the crack may produce an effect on the propagation path which cannot be considered in our model, where the fluid dynamics is neglected. The effect of viscosity on the path of a fluid-filled crack has never been addressed by either numerical models or analogue experiments. Therefore, we cannot rule out that our simulated paths are affected by errors related to the "quasi-static" approach used in our model.

– *Non-elastic effects and boundaries*: Our numerical model makes use of dislocation solutions for an elastic medium. Non-elastic effects which may take place at the tip of the crack, where the elastic theory prescribes unbounded stress concentration, are therefore neglected.

We consider the effect of the boundaries of the gelatin container when computing the external stress due to the loading within the gelatin block. However, such an effect is not taken into account when computing the opening of the fluid filled crack. This may affect both the internal overpressure and the stress perturbation induced by the fluid-filled crack. Rigid boundary conditions for a finite block of gelatin may be implemented with the BE approach, and this could represent a step forward for the comparison between laboratory experiments and simulations.

The external stress field due to the loading is computed with an FE model for an elastic and homogeneous gelatin block. This represents an improvement with respect to previous studies that neglected the effect of rigid boundaries. However, non-elastic effects and possible inhomogeneities of the gelatin block (for instance, the strengthening of the free surface due to the drying of the surface of the gelatin block), may further reduce the intensity of the loading stress.

– *Experimental conditions*: Errors in estimating the initial parameters of fluid-filled crack (initial length, position, dip angle, and overpressure), or the elastic parameters of the gelatin block, may also affect our comparison. However, they would not justify the systematic observation of greater deflection for the simulated paths with respect to the experiments. The systematic lesser deflection of the air-filled crack may be partially caused by difference in the strike angles: any strike direction different from zero (which is parallel to the long edge of the loading plate) may contribute to a lesser intensity of the external stress field experienced by the air-filled crack. In order to check this effect we run a simulation of exp34, which has the best strike angle (Fig. 8). The numerical simulation is still more deflected, however, the experimental and numerical trajectories seem closer than exp61 (Fig 7a), which also has $\delta >> \delta_c$.

In addition, several deflection experiments (up to 5) were performed within the same gelatin block, by varying the injection point (and the loading position, accordingly). The effect of pre-existing cuts within the gelatin block, due to the propagation of previous air-filled cracks, as well as the effect of the cut gelatin behind the air-filled crack, is not considered in the numerical model. Pre-existing cuts may interact with both the loading stress and the crack induced stress (*Le Corvec et al., 2013*). In general, we did not propagate air-filled cracks in the close vicinity of the paths of previous intrusions, which were always at a distance larger than 0.5·L (half crack length), except for exp45 and exp60, which started with an initial distance of 0.36·L and 0.44·L from the previous intrusions, respectively. Note also, that in order to reduce the effect of pre-cuts on the loading stress field, we always avoided having previous crack-paths cutting the gelatin block between the loading mass and the propagating air-filled crack.

Finally, it is worth highlighting that the initial dip angle also have an influence on the trajectory. This is due to two effects: first, the different shear stress experienced by the cracks with slightly different dip angles; second, an air-filled crack which started with an outward dipping angle with respect to the load, would tend to propagate towards less intense external shear stress, with respect to a crack starting with inward dipping angle. Considering the range of initial dip angle deviations of our experiments (±3.5°), we computed the corresponding variations of the shear stress on inclined air-filled cracks (τ), we obtained: $|\tau^{(+3.5°)} - \tau^{(-3.5°)}| / \sigma_{xz} = 0.22$. Using these shear stress values to compute δ, we obtain: $|\delta^{(+3.5°)} - \delta^{(-3.5°)}| / \delta^{(0°)} = 0.14$ (for these calculations we used the stress field from the FE model, the air-filled crack parameters from exp59, and we varied the initial dip angle).

However, the initial dip angle deviations of air-filled cracks were always taken into account when performing the numerical simulations of experiments, and therefore they do not affect the difference in the simulated vs experimental trajectories.

– *Transient loading stress*: When placing the loading mass on the surface of the experiment, we observed oscillations of the gelatin block. This can be seen, for instance, in the trajectory recorded for exp29 (Fig.5d), for which the loading mass was rather heavy. The effect of an oscillating stress field on the air-filled crack is not considered in the numerical model, and may actually contribute to a delayed or emergent response of the air-filled crack to the application of the loading.

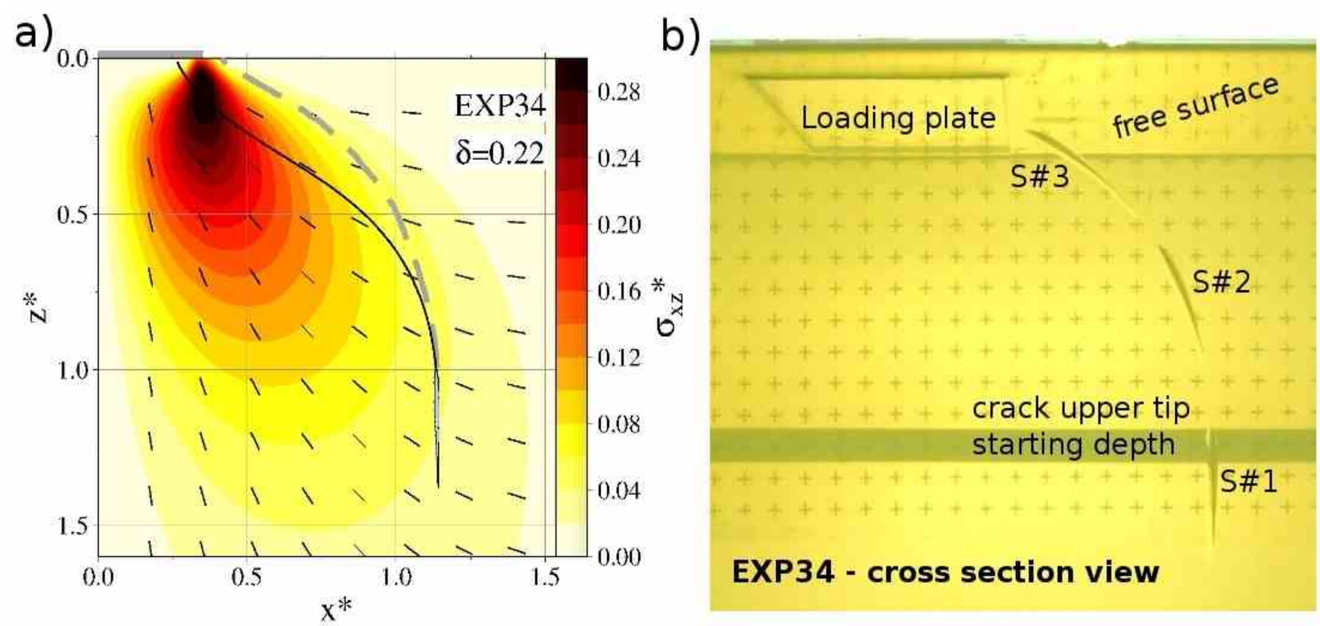

Figure 8: *Panel a) Numerical simulations of exp34. Symbols and colour contour are the same as in Fig 7. b) Cross section view of exp34. Three snapshots (S#1 - S#2 - S#3) of the air-filled crack during the deflection experiment are superposed on the same background image.*

4.2 Evaluating δ for inclined dikes, horizontal sills, and lateral magmatic intrusions

In the current study we always considered fluid-filled cracks starting vertically oriented, and propagating upwards. Therefore, the shear stress component of the external stress σ_{xz}, (with *x*-axis horizontal and *z*-axis vertical) represents the shear stress acting on the crack plane in the direction of propagation. Similarly, if a fluid-filled crack is not vertical, and/or its direction of propagation is out of the *xz*-plane, the one possible choice to compute δ will be to consider $\sigma_{x'z'}$, with x' perpendicular to the crack plane, and z' along the direction of propagation. Also, the absolute value of $\sigma_{x'z'}$ should be considered, since negative shear stress values would still contribute to the fluid-filled crack deflections (in the opposite direction). However, using $\sigma_{x'z'}$ for computing δ has some implications that should be carefully considered:

1) If a propagating fluid-filled crack is oriented perpendicular to the direction of maximum compression, it would experience $\sigma_{x'z'} = 0$, and therefore $\delta = 0$, implying $\delta < \delta_c$ and no deflection would be expected. However, this might be an unstable equilibrium situation: if the magnitude of the background stress is large enough, as soon as the crack tip orientation, or the principal stress direction, slightly changes (for instance due to small heterogeneities of the host material or in the external stress field) δ would increase and the fluid-filled crack may start deviating towards the direction of maximum compression. This can be observed in laboratory experiments such as *Menand (2010)*, and reproduced with BE numerical simulations by adding a small perturbation to the direction of propagation (*Maccaferri et al., 2011*).

2) Using $\sigma_{x'z'}$, δ values lower than the critical range δ_c may actually indicate two different conditions: i) similarly to what described above, the crack is oriented in the direction perpendicular to minimum compression (therefore $\sigma_{x'z'}$ is close to zero), but the background stress field is actually large enough to affect the dike path, for other crack orientations; ii) the crack is not oriented perpendicular to the minimum compression, but the effect of background stress is negligible. In both cases we should not expect deflection. However in the first case the crack would keep on following the background stress direction (which may change during propagation), while in the second case the crack would propagate straight, even if the principal stress orientation due to the background stress changes.

In order to resolve these ambiguities one may chose to consider the maximum background shear stress acting at the tip of the crack, σ_{xz}^{max}, instead of $\sigma_{x'z'}$. In this way values of δ lower than the critical range, would always indicate that the effect of the background stress on the propagation path is negligible, and value of δ larger than the critical range would indicate that the principal stress direction due to the background stress dominates over the stress change induced by the intrusion. Notice also that our estimate for the critical range of δ values can apply also to a definition of δ based on σ_{xz}^{max}, $\delta=(\sigma_{xz}^{max}/Dp)/L^*$. In fact, for our geometrical set-up, at the beginning of the deflection experiment $\sigma_{xz}^{max}\approx\sigma_{xz}$, because the the principal background-stress direction at the tip of the crack is ~45°.

In addition, it has to be noticed that the criterion for fluid-filled crack deflection which we introduced here (as well as the one previously proposed by *Watanabe et al., 2002*), may be applied (or updated) at any point of the propagation path. In fact, during propagation, δ may change because of an heterogeneous external stress field and/or because of changes in the fluid overpressure and crack length. As an example, we computed δ (using both, σ_{xz}^{max} and $\sigma_{x'z'}$) along the paths of the numerical simulations of exp44, 59, and 61 (Fig. S2).

With these specifications, our criterion for deflection may be applied also to horizontal sills, inclined dikes, and lateral intrusions, which are common in many volcanic settings. In some cases, magma overpressure may not be due to buoyancy, as in our experiments and simulations, but provided by hydraulic connection with a magma chamber and/or lateral stress gradients in the external stress field, this also should be taken into account when computing δ. With this respect, we did not test our results for fluid-filled fractures with highly non-linear overpressure profile (which may be due for instance to the presence of both gas and liquid phases within the crack), in such case the average magma overpressure and the crack length may relate to the stress change induced by the crack differently, with respect to our experiments and simulations, so that the the critical range δ_c may also change.

5 Conclusions

We revised the critical ratio R_c for fluid-filled crack deflection as computed by *Watanabe et al. (2002)*. We show that the effect of the rigid boundaries of the gelatin container are not negligible and that the use of analytical formulas to estimate the experimental critical ratio for deflection leads to an overestimation of R_c. By using 3D FE model to compute the loading stress field within the gelatin block, and accounting for the boundary effects, we estimate R_c = 0.09 (the previous estimate, based on analytical formulas, was R_c = 0.2) where $R = \sigma_{xz}/Dp$, meaning that the magma path becomes sensitive to the external stress field when its deviatoric component reaches one tenth of the magma driving overpressure. We also confirmed that the propagation path of a fluid-filled crack does not depend solely on the competition between the external stress (σ_{xz}) and the internal overpressure (*Dp*), but also on the length of the crack (*L*), which influences the magnitude of the stress field induced by the crack (this has been postulated by previous theoretical studies such as *Cotterell and Rice, 1980*). We showed that given the same *R*, propagation paths depend on *L*, with a more reduced influence of the external stress field for longer dikes. Therefore we propose the definition of a new parameter to characterize the deflection of fluid-filled cracks using the dimensionless parameter $\delta = R / L^*$. We estimated a critical range of δ values, $\delta_c = [0.04; 0.18]$ from our numerical simulations, close to the one determined from our laboratory experiments $\delta_c = [0.06; 0.22]$ (which are also consistent with previous experiments from *Watanabe et al. 2002*).

The critical range for deflection we present here defines under what conditions the path of a fluid-filled crack can be directly derived from a stress model: when $\delta > \delta_c$ the crack is expected to follow closely the direction perpendicular to the less compressive axis of the background stress field; when $\delta < \delta_c$ it is expected to propagate straight. Indeed, elaborate models for fluid-filled crack propagation are required within the range of critical δ values ($\delta \in \delta_c$), provided that the calculation of δ is updated along the path of the intrusion. This has implications for studies addressing magmatic dike propagation paths given the stress field acting at a volcano. For laterally propagating dikes over long distance, as often observed in rifting area, the influence of the external stress field on the propagation path will depend on the balance between the increasing dike length and the pressure drop due to magma withdraw from the magma chamber, so that a progressively larger effect of the background stress (which would be expected by neglecting the effect of the dike length and accounting for the magma pressure drop solely), would not necessarily occur, and should be examined in each circumstances. Last, for research intended to address the propagation path and the rising velocity of magmatic intrusions (e.g. *Pinel et al., 2017*), our results shows that the length of the intrusion should be taken into account in order to evaluate whether the direction of maximum compressive stress defines the propagation path of the intrusion.

Acknowledgments:

We thank the Editor – Claudio Faccenna – the Associate Editor, and the Reviewers – Meredith Townsend, and an anonymous Reviewer – for their constructive comments that substantially contributed shaping this article. The collaboration between ISTerre and GFZ was funded by the Campus France-DAAD exchange program. Part of the work done by FM to develop further the boundary element code was founded by BMBF, within the framework of the project SECURE.

All data plotted in the manuscript and used for our analysis are attached as a supplementary file.

References

Bagnardi, M., Amelung, F., Poland, M.P., (2013), A new model for the growth of basaltic shields based on deformation of Fernandina volcano, Galapagos Islands. *Earth Planet. Sci. Lett.* 377–378, 358–366.

Bonaccorso, A., Currenti, G., Del Negro, C., Boschi, E., (2010), Dike deflection modelling for inferring magma pressure and withdrawal, with application to Etna 2001 case. *Earth and Planetary Science Letters* 293, 121–129.

Corbi, F., Rivalta, E., Pinel, V., Maccaferri, F., Bagnardi, M., Acocella, V., (2015), How caldera collapse shapes the shallow emplacement and transfer of magma in active volcanoes, *Earth and Planetary Science Letters* 431, 287 – 293, doi:10.1016/j.epsl.2015.09.028.

Corbi, F., Rivalta, E., Pinel, V., Maccaferri, F. and Acocella, V., (2016), Understanding the link between circumferential dikes and eruptive fissures around calderas based on numerical and analog models. *Geophysical Research Letters*, *43*(12), pp.6212-6219.

Cotterell, B., and J. R. Rice (1980), Slightly curved or kinked cracks, *Int. J. of Fracture*, 16, 155-169.

Dahm, T., (2000a), Numerical simulations of the propagation path and the arrest of fluid-filled fractures in the Earth. *Geophysical Journal International*, 141(3), pp.623–638.

Dahm, T., (2000b), On the shape and velocity of fluid-filled fractures in the Earth. *Geophys. J. Int*. 142, 181–192.

Delaney, P. T., D. D. Pollard, J. I. Ziony, and E. H. McKee (1986), Field relations between dikes and joints: Emplacement processes and paleostress analysis, *J. Geophys. Res.*, 91(B5), 4920-4938, doi:10.1029/JB091iB05p04920.

Fukushima, Y., Cayol, V., Durand, P. and Massonnet, D., (2010), Evolution of magma conduits during the 1998–2000 eruptions of Piton de la Fournaise volcano, Réunion Island. *Journal of Geophysical Research: Solid Earth*, *115*(B10).

Grandin, R., et al. (2009), September 2005 Manda Hararo-Dabbahu rifting event, Afar (Ethiopia): Constraints provided by geodetic data, *J. Geophys. Res.*, 114, B08404, doi:10.1029/2008JB005843.

Griffith, A., (1920), The phenomena of rupture and flow in solids. *Philosophical Transac- tion of the Royal Society Series* A 221, 163–198.

Heimisson, E.R., Hooper, A. and Sigmundsson, F., (2015), Forecasting the path of a laterally propagating dike. *Journal of Geophysical Research: Solid Earth*, *120*(12), pp.8774-8792.

Jaeger, J.C., Cook, N.G. and Zimmerman, R., (2007), *Fundamentals of rock mechanics*. 4th ed., Blackwell Publishing, Oxford. ISBN 978-0-632-05759-7.

Kavanagh, J.L., Menand, T. and Daniels, K.A., (2013), Gelatine as a crustal analogue: Determining elastic properties for modelling magmatic intrusions. *Tectonophysics*, *582*, pp.101-111.

Le Corvec, N., Menand, T. & Lindsay, J. Interaction of ascending magma with pre-existing crustal fractures in monogenetic basaltic volcanism: an experimental approach. *J. Geophys. Res. Solid Earth* 118, 968–984 (2013).

Lister, J. R., (1990) Buoyancy-driven fluid-filled fracture: The effects of material toughness and of low viscosity precursors, *J. Fluid Mech.*, 210, 263-280.

Maccaferri, F., Bonafede, M. and Rivalta, E., (2011), A quantitative study of the mechanisms governing dike propagation, dike arrest and sill formation. *Journal of Volcanology and Geothermal Research*, 208(1–2), pp.39–50.

Mériaux, C., J. R. Lister, J., R., (2002) Calculation of dike trajectories from volcanic centres, *J. Geophys. Res.* 107(B4) (2002) 1–10. doi:10.1029/2001JB00436

Menand, T., Daniels, K.A., Benghiat, P., (2010), dike propagation and sill formation in a compressive tectonic environment. *Journal of Geophysical Research* 115, B08201.

Nakamura, K., K. H. Jacob, and J. N. Davies (1977), Volcanoes as possible indicators of tectonic stress orientation, Aleutians and Alaska, *Pure Appl. Geophys.*, 115, 87-112.

Peltier, A., V. Ferrazzini, T. Staudacher, and P. Bachélery (2005), Imaging the dynamics of dyke propagation prior to the 2000– 2003 flank eruptions at Piton de La Fournaise, Reunion Island, *Geophys. Res. Lett.*, 32, L22302, doi:10.1029/2005GL023720.

Pinel, V., Jaupart, C., (2004), Magma storage and horizontal dyke injection beneath a volcanic edifice. *Earth and Planetary Science Letters* 221, 245-262.

Pinel, V., Carrara, A., Maccaferri, F., Rivalta, E. and Corbi, F., (2017), A two-step model for dynamical dike propagation in two dimensions: Application to the July 2001 Etna eruption. *Journal of Geophysical Research: Solid Earth*, *122*(2), pp.1107-1125.

Pollard, D. D., Townsend, M. R. (2018), Fluid-filled fractures in Earth's lithosphere: Gravitational loading, interpenetration, and stable height of dikes and veins, *Journal of Structural Geology*, Volume 109, pp 38-54.

Rivalta, E., Taisne, B., Bunger, A.P. and Katz, R.F., (2015) A review of mechanical models of dike propagation: Schools of thought, results and future directions. *Tectonophysics*, *638*, pp.1-42.

Roman, A. and Jaupart, C., (2014). The impact of a volcanic edifice on intrusive and eruptive activity. *Earth and Planetary Science Letters*, *408*, pp.1-8.

Roper, S., Lister, J., (2007), Buoyancy-driven crack propagation: the limit of large fracture toughness. *J. Fluid Mech*. 580, 359–380.

Rubin, A.M., and D. D. Pollard (1987), Origins of blade-like dikes in volcanic rift zones, *U.S. Geol. Surv. Prof. Pap.*, 1350, 1449-1470.

Segall, P., (2010), Earthquake and volcano deformation, Princeton University press, Princeton.

Sigmundsson, F. et al. (2015) Segmented lateral dyke growth in a rifting event at Bardarbunga volcanic system, iceland. *Nature* 517, 191–195.

Toutain, J.-P., P. Bachelery, P.-A. Blum, J. L. Cheminee, H. Delorme, L. Fontaine, P. Kowalski, and P. Taochy (1992), Real time monitoring of vertical ground deformations during eruptions at Piton de la Fournaise, *Geophys. Res. Lett.*, 19(6), 553– 556.

Townsend, M. R., M. R., Pollard, D. D., Smith, R. P., (2017) , Mechanical models for dikes: A third school of thought, *Tectonophysics*.

Watanabe, T., Masuyama, T., Nagaoka, K., Tahara, T., (2002), Analog experiments on magma-filled cracks: competition between external stresses and internal pressure. *Earth Planets Space* 54, 1247–1261.

Weertman, J., (1971) Theory of water-filled crevasses in glaciers applied to vertical magma transport beneath oceanic ridges. *Journal of Geophysical Research*, 76, pp.1171–1183.